The Astrophysical Journal, 221:436–448, 1978 April 15

TWIN BEAM MODELS FOR DOUBLE RADIO SOURCES. II. DYNAMICAL CALCULATIONS

Paul J. Wiita
Joseph Henry Laboratories, Princeton University; and
Enrico Fermi Institute, University of Chicago
Received 1977 January 31; accepted 1977 July 13

ABSTRACT

Numerical experiments on continuous ejection models for symmetric double radio sources (constructed along the lines of Blandford and Rees) are performed. The equations for relativistic spherical flow and for nonrelativistic aspherical expansion are derived after a discussion of the physical conditions in both the internal plasma and the confining gas cloud is given. These coupled evolution equations are nondimensionalized, and a scaling law relating configurations of the same reduced luminosities is posited. Models for different values of internal luminosity, and for variations in the parameters of the external gas (size, density, temperature, shape), are computed, and the scaling law is verified. The most important variables turn out to be the dimensionless luminosity and the eccentricity of the confining cloud. Low-power models tend to form bubbles: the expanding blob of plasma bifurcates. Stronger sources lead to oppositely directed jets that sometimes attain relativistic expansion velocities. We also find that the flatter the cloud, the sooner bubbles form.

Subject headings: galaxies: structure — hydromagnetics — radio sources: general

I. INTRODUCTION

Twin beam, or continuous ejection, models for double radio sources provide a reasonably coherent and consistent explanation of the bulk of the observations of such objects. Variants of this theory have been proposed by several authors over the last few years (Rees 1971; Longair, Ryle, and Scheuer 1973; Scheuer 1974; Blandford and Rees 1974 [hereafter BR]; Wiita 1976). In a previous paper (Wiita 1978, hereinafter Paper I) the steady-state twin exhaust model of BR was reanalyzed and extended to new regimes. In particular, the possible existence of hotter, denser confining gas clouds was investigated in Paper I. Such configurations seem to provide a better fit to recent VLBI measurements on the alignment of small nuclear sources with the extended radio lobes (cf. Kellermann *et al.* 1976).

But the fact that a steady-state solution to a hydrodynamics problem has been shown to exist certainly does not guarantee that it can actually be established starting from plausible initial conditions. Thus, the demonstration that the twin-exhaust picture, as expounded in BR and Paper I, is a quasi-stationary final configuration for certain reasonable physical parameters, leads us to desire to investigate the dynamics of the model more fully. It is the aim of this paper to start such an analysis, stressing Newtonian numerical calculations. We have not performed full two- (or three-) dimensional hydrodynamic calculations; rather, these results refer to the integration of the equations of motion for the shell forming the boundary between the external confining gas and the internal fluid. A special-relativistic treatment which would be valid at times later than those considered here has been presented elsewhere (Wiita 1976). So far, however, the numerical experiments have not been extended to that dominantly one-dimensional, but relativistic, regime.

In our calculations, we assume that at an initial time a source of relativistic plasma is turned on in a galactic nucleus, and that its power remains constant thereafter. The plasma is confined by a somewhat flattened gas cloud (see BR and Paper I for details on the constituents of the inner and outer fluids) which is also taken to reside in the nucleus, but which trails off in a bi-Gaussian fashion (eq. [6], Paper I) until a low intergalactic density is reached. In § II, some of the important physical assumptions and approximations employed will be discussed; they set a limit on the validity of this work.

At the early stages the flow is relativistic, but nearly spherical, since the ram pressure differences between the polar and equatorial directions are negligible until the blob of plasma attains a radius greater than $0.1l$ (l is the average scale height for the confining gas). By the time asphericity rears its head, the velocity of the boundary is sufficiently subrelativistic that Newtonian equations of motion can be utilized. During this period, the internal pressure can be rather accurately treated as a function of time alone because the sound speed ($c/\sqrt{3}$) is much greater than boundary velocities and pressure differentials are rapidly smoothed out. However, this constant-pressure assumption breaks down if the boundary starts to expand too rapidly, so that the internal sound speed is no longer very much greater than the wall's velocity; it also is no longer true if the changing shape of the wall induces large internal velocities, regardless of the magnitude of the motion. Our *Ansatz* may also fail if the pinching of the neck stresses the fact that the energy and plasma source is concentrated at the center. Clearly, the Newtonian wall motion approximation also fails then, and in nearly every case these failures occur with small separations in time between them. If the situation at that time is such that the cavity is elongated to the extent that the flow is predominantly longitudinal (along the channels), then the internal fluid can be described by just two variables: its pressure or internal energy density, and its velocity. The coupling of this space- and time-dependent internal flow to the motion of the boundary between it and the confining fluid becomes the crux of the problem at this later stage.

In § IV we give the results of our numerical calculations in tabular and graphical form. We find that jets are formed only for fairly strong sources, and—contrary to the speculation of Rees (1976)—we obtain bubbles as the more likely outcome for weak ones, even if turned on abruptly. We suggest new areas for theoretical work and summarize our conclusions in § V.

II. PHYSICAL ASSUMPTIONS AND APPROXIMATIONS

We note that if a source of the luminosities considered in Paper I ($L \sim 10^{46}$ ergs s^{-1}) is suddenly turned on, the plasma it emits starts its expansion at high velocities, substantially supersonic with respect to the external medium (e.g., in the basic BR model for Cygnus A: $T \sim 3 \times 10^8$ K, $n_0 \sim 4 \times 10^2$ cm^{-3}, $l \sim 135$ pc). The first approximation we employ is to assume an axisymmetric evolution. Although the initial velocity is determined by the original arbitrary overpressure in the small volume from which the plasma starts expanding, the motion is quickly dominated by the power of the source and the properties of the ambient gas.

The magnetic field is not considered explicitly; rather, in this treatment, the energy it carries acts just like the relativistic particles in the interior fluid. (Its pressure, if the fields are roughly isotropic, is one-third its energy density also.) It is certain that this neglect of magnetic effects is of some importance, particularly in regard to the development of Kelvin-Helmholtz instabilities which may be strong near the nozzle and at the head of the beam. For fuller discussions of this problem, see Blake (1972), Turland and Scheuer (1976), Blandford and Pringle (1976), and Ferrari, Trussoni, and Zaninetti (1977). However, for computational simplicity, we provisionally accept the argument of BR that the streaming instabilities are limited by nonlinear effects, and act upon the beam only as rapid but small fluctuations in its shape and position.

The analysis of Rayleigh-Taylor instabilities mentioned in Paper I purported to show that if the exhaust configuration is established, then it is most likely stable against such perturbations. But during the dynamical motions of the formation epoch such modes are almost certainly excited, as the time scales for growth of the disturbances are of the same order as the expansion time for the blob of ejected plasma. Such instabilities are implicitly included in a correct dynamical formulation, and, if at all important, ought to be excited by the inherent inaccuracies of a discrete, numerical code; we will see their influence on the numerical experiments displayed in § IV.

Also, the radiation emitted by the plasma itself and by the shocked fluid it sweeps up will be ignored. Naturally, some of the same mechanisms proposed by BR to explain the eventual synchrotron radiation from the hot spots will be working even at these stages, and the losses may be significant. In the case of supernova shocks penetrating the interstellar medium, the energy lost by radiation is quite large (e.g., Chevalier 1974); but other relevant work on physical conditions more closely comparable to the ones we use indicates lesser losses (Bollea and Cavaliere 1976). Our basic equations for the dynamics do not include radiation terms for either energy or momentum transport. This is a major *Ansatz*, already implying 10% to 20% uncertainties in the computed values; however, it should be noted that such effects are crudely modeled in our numerical work, which allows for variations in the amounts of kinetic and internal energy in the boundary region.

Another major aspect we neglect is turbulence. While arguments can be given for the likelihood of the flow to be roughly "laminar" (cf. BR), they are not thoroughly convincing. But a strong reason for not trying to include plasma turbulence is that the manner in which it could be generated, as well as reasonable equations giving its evolution, are problematical. It should be noted that Gull and Northover (1973) invoke turbulence (qualitatively) in their giant bubble model in attempting to explain the hot spots. This neglect is a major restriction on the accuracy of our results.

A further important approximation is that the exterior gas that is shocked by, and then swept along with, the expanding plasma cloud forms a relatively thin shell. This is possible as long as the shock is a strong one; i.e., the speed at which the boundary advances must be much greater than the sound speed of the external gas, for then both the density and temperature of the material are increased considerably. This shocked fluid then meets the internal fluid at what could be roughly described as a contact discontinuity; however, some mixing of the external fluid into the relativistic plasma is expected. This phenomenon, like the entrainment of the external plasma BR mention, can clearly be of importance, but it is very difficult to model well and will be ignored in our work. Even when the shock is strong, we probably only get genuinely thin shells and the real "snowplow" effect if the heated material cools off fast enough to increase its density further (Spitzer 1968). This is *not* likely in our case, since the shocked gas is too hot to cool; by this we mean that at these high temperatures and densities the radiation that is likely to be emitted (Cox and Tucker 1969; Cox and Daltabuit 1971) cannot drop the temperature quickly enough to enhance the density increase very much. While we are neglecting the explicit dynamical importance of the magnetic fields, we ought to note that they will, in all probability, help keep the boundary layer thinner than it would otherwise be (BR).

Related problems should also be mentioned. As the evolution proceeds, the expansion often becomes subsonic in some directions, especially those associated with the equatorial plane. Then the plasma is no longer sweeping up a shell of fluid via the shock; instead it is pushing outward like a bubble, and its influence propagates outward into the surrounding medium at its speed of sound, hence ahead of the actual boundary. The evolution is estimated by taking that portion of the shell to be no longer accreting mass, and by ignoring the external density wave which really could not be properly included except by employing a full two-dimensional hydrodynamics code. Further, the velocity of the actual boundary between the relativistic fluid and the shocked gas is always less than that of the advancing shock front; for strong nonrelativistic shocks in a monatomic gas the velocity of this discontinuity lags that of the shock front by about 25% (Landau and Lifshitz 1959). Thus, we are really dealing with a wall that could have a substantial thickness, one on the order of one-fourth of the total dimensions of the blob. Zel'dovich and Raizer (1966) show that an analogous thin shell approximation in the context of a spherically symmetric strong explosion is quite accurate. Modifications of this approach in exponential atmospheres are also discussed in Zel'dovich and Raizer (1966). Sakashita (1971) followed an explosion-generated shock front, restricted to locally radial motion, but Bhowmick (1975) showed that in that case the shell did not stay thin for very long. So this probably implies nonnegligible errors for our work, which, however, may be ameliorated by our treatment of the energy balance at the shock, and by the magnetic field.

III. DYNAMICAL EQUATIONS

a) *Spherical Expansion*

For the spherical geometry applicable to the earliest stages of the development we must use relativistic equations for the boundary motion. As we have mentioned earlier, the internal pressure (or energy density) can be taken as a function of time alone during this time period. Under these limitations we can present the boundary motion equations. Let X be the radius of the blob of plasma and (in the laboratory frame) let $U = dX/dt$; then $dM/dt = 4\pi X^2 \rho_1 U$ and

$$M\frac{dU}{dt} = 4\pi\gamma^{-1}X^2(p - p_1) - 4\pi\gamma^{-2}X^2\rho_1 U^2\,, \tag{1}$$

where M is the total mass swept up and ρ_1 and p_1 are the mass density and pressure of the external gas; p is the pressure of the internal plasma.

The basic equation for the change of the pressure is determined by an input from the central energy source of strength L (in the laboratory frame), which is distributed between the energy of the relativistic fluid and the energy of the shell making up the boundary. For the case of a fully relativistic internal fluid, and as long as the motion of the walls is not extremely relativistic (i.e., γ is not $\gg 1$, a condition we always satisfy), then the energy supplied to the external medium is roughly (Blandford and McKee 1976)

$$E_{\rm sup} \approx 3Lt/(8\gamma^2)\,. \tag{2}$$

Thus the total energy balance can be written as

$$L = \frac{dE}{dt} = \frac{d}{dt}\int \rho dV + \frac{d}{dt}(E_{\rm sup})\,. \tag{3}$$

Because $V = (4/3)\pi X^3$ and $\rho = 3p$ is a constant over the volume at a given time, we can insert equation (2) into equation (3) to obtain

$$L = 12\pi p X^2 U + 4\pi X^3\frac{dP}{dt} + 3L/(8\gamma^2) - \tfrac{3}{4}LtU\frac{dU}{dt}\cdot \tag{4}$$

We solve equation (4) for dP/dt and equation (1) for dU/dt and find the following system of differential equations:

$$\frac{dU}{dt} = 4\pi X^2[p - p_1 - \rho_1 U^2\gamma^{-1}](M\gamma)^{-1}\,, \tag{5}$$

$$\frac{dP}{dt} = \frac{L[1 - \frac{3}{8}\gamma^{-2} + \frac{3}{4}tU(dU/dt)] - 12\pi X^2 Up}{4\pi X^3}\,, \tag{6}$$

$$\frac{dX}{dt} = U\,. \tag{7}$$

These equations are then integrated from the following initial conditions: a constant L is chosen, and an initial radius, $X_0 \sim 0.01l$ is also picked; an initial internal pressure is also selected ($\sim 300p_0$, where p_0 is the central pressure for the confining gas). This gas also requires, for its complete specification, a temperature (or density) to be given along with an equation of state. For details on such a cloud and its stability, see Paper I. The initial velocity is taken as (after Landau and Lifshitz 1959)

$$U(t_0) = \beta_s\left[\frac{(\Gamma - 1)}{2\Gamma} + \frac{(\Gamma + 1)p(t_0, X_0)}{2\Gamma p_1(t_0, X_0)}\right]^{1/2},$$

where $p_1(t_0, X_0) \approx p_0$ and β_s is the speed of sound in the external gas, $\beta_s = (\Gamma p_1/\rho_1)^{1/2}$; Γ is the adiabatic index.

As mentioned above, this spherical approximation is reasonable until X reaches about one-tenth of the scale height; when this, or some other preselected radius, is exceeded, this integration scheme is halted, and the current values of X, U, p, and t are used to initialize the axisymmetric integration described in the next section. The actual choice of $p(t_0, X_0)$ does not greatly influence either the pressure or the time at which the desired radius is reached: differences of a factor of 10 in that overpressure are swamped by the energy provided by the L term and produce variations in p or t of around only 10%. In the same manner, the actual value of X_0 is quite unimportant until it gets to be about a third of the radius at which this spherical advance is terminated. The actual integration of equations (5)–(7) (plus the change in mass equation) is carried out using a fourth-order Runge-Kutta scheme with a variable step size that attempts to increase itself at every time step (Gear 1971, § 5.4) as long as the values computed using both the current and the increased time step agree to a certain tolerance; if they do not, the step size is repeatedly cut until these differing values for the results of the integration are in sufficiently close agreement.

b) *Axisymmetric Evolution*

Once the initial expansion has passed $0.1l$, the velocity of the shock is invariably under $0.2c$, and relativistic corrections to the boundary motion are small. We still assume that internal pressure gradients are small, and then we have, for a segment of the boundary of surface area da and mass m located at Z, and of radius R, this relation for the increase in mass of that wall segment:

$$\frac{dM}{dt} = da\rho_1(R, Z)(U^R \cos\theta + U^Z \sin\theta), \tag{8}$$

where $U^R = dR/dt$, $U^Z = dZ/dt$, and θ is the angle between the Z-axis and the plane of this boundary element. The Newtonian equations of motion are:

$$\begin{aligned} \frac{dU^Z}{dt} &= \frac{da}{m}[(p - p_1)\sin\theta - \rho_1 U^Z(U^R\cos\theta + U^Z\sin\theta)], \\ \frac{dU^R}{dt} &= \frac{da}{m}[(p - p_1)\cos\theta - \rho_1 U^R(U^R\cos\theta + U^Z\sin\theta)]. \end{aligned} \tag{9}$$

This pair of equations is easily interpreted: p is the internal fluid pressure pushing outward and tending to accelerate the boundary, p_1 is the varying external thermal pressure opposing this acceleration, and the last terms represent the ram pressure. (For the special-relativistic generalization of eqs. [8] and [9], see § IV.4 of Wiita 1976.)

Now we must note that the assumption that the shock is strong, which allows equation (2) to be used, may no longer hold. In fact, we will see that eventually, for at least some portions of the interface, a shock ceases to exist as the expansion becomes subsonic, and even reverses itself into a contraction. One method, the quasi-radial approach pioneered by Lumbach and Probstein (1969) and applied by several others (Sakashita 1971; Möllenhoff 1976; see Wiita 1976 for a critique of this technique), would be adequate for the beginning of the next stage of the calculation, but is not so useful for the later, wholly aspherical development.

Here we try another general attack, and determine the equation for the change in pressure via the energy inserted by the central source and that taken up by the shell consisting of the swept-up external fluid. There are two basic contributions to the energy of the boundary layer (neglecting radiation): the kinetic (going like MU^2) and the internal (W). Write this balance as (cf. eq. [3])

$$L = \frac{dE}{dt} = \frac{d}{dt}\int \rho dV + \frac{d}{dt}(MU^2/2 + W). \tag{10}$$

The final term, referring to the internal energy, is a complicated one, depending in detail upon the previous history of the swept-up fluid as well as its composition. As the external gas passes through the shock, its temperature and density both increase rapidly; when the shock is sufficiently strong, the assumption that this material takes up only a rather small fraction of the total volume of the blob is a reasonable one (§ II).

Basically, the increases in kinetic and internal energy are of the same order of magnitude, and close to proportional. Our key approximation will be to formalize such a proportionality and ignore its time dependence by expressing the total energy supplied to the external medium as merely a constant factor multiplying the well-defined kinetic energy, i.e.,

$$(MU^2/2 + W) \approx \alpha(MU^2/2)\,. \tag{11}$$

Rough upper (~ 4) and lower (25/16) bounds can be set on α (Wiita 1976), by using shock jump conditions; physically a larger α corresponds to thicker walls. While this might appear to be a major, and perhaps crude, approximation, the value of α actually makes very little difference in the size and shape of specific configurations, as confirmed by many spherical and axisymmetric integrations (cf. § IV).

While we will not bother to do so explicitly for the spherical equations, we shall now remove the dimensional factors from the Newtonian, axisymmetric equations, and will cast them into the discrete form necessary for computer evolution. The velocities have already been effectively nondimensionalized as we have been taking $c = 1$ in this section. All other variables can be divorced from their physical corequisites in the following manner. Let the subscript i refer to the ith zone into which the boundary layer is divided, and define

$$r_i = R/l\,, \quad z_i = Z/l\,, \quad \tau = ct/l\,, \quad \mathscr{L} = L/(p_0 c l^2)\,, \quad \psi = p_1(r, z)/p_0\,, \quad \chi = p(\tau)/p_0\,,$$
$$da_i = (\text{area of } i\text{th zone})/l^2\,, \qquad m_i = (\text{mass of } i\text{th zone } c^2)/(p_0 l^3)\,.$$

Using the definition of the sound speed and dividing equation (8) by $p_0 l^2/c$ leads to the discrete mass increase equation

$$\frac{dm_i}{dt} = da_i(U_i^z \sin\theta_i + U_i^r \cos\theta_i)\frac{\Gamma}{\beta_s^2}\psi(r, z)\,. \tag{12}$$

Overall division of equation (9) by c^2/l leads to the reduced acceleration equations:

$$\begin{aligned}\frac{dU_i^z}{d\tau} &= \frac{da_i}{m_i}[\chi - \psi(r, z)]\sin\theta_i - \frac{U_i^z}{m_i}\frac{dm_i}{d\tau}\,,\\ \frac{dU_i^r}{d\tau} &= \frac{da_i}{m_i}[\chi - \psi(r, z)]\cos\theta_i - \frac{U_i^r}{m_i}\frac{dm_i}{d\tau}\,.\end{aligned} \tag{13}$$

The final basic equation comes from equation (10) with the approximation (11) included:

$$L \approx 3V\frac{dp}{dt} + 3p\frac{dV}{dt} + \frac{\alpha}{2}\frac{d}{dt}(MU^2)\,,$$
$$MU^2 \approx \sum_i m_i[(U_i^r)^2 + (U_i^z)^2] \equiv \sum m_i U_i^2\,.$$

If we divide by $p_0 c l^2$, solve for the derivative of the pressure, and make use of reflection symmetry about the equatorial plane, we obtain the key result

$$\frac{d\chi}{d\tau} = \frac{1}{\mathscr{V}}\left\{\frac{\mathscr{L}}{6} - \chi\frac{dV}{d\tau} - \frac{\alpha}{6}\left[\frac{d(\sum m_i U_i^2)}{d\tau}\right]\right\}, \tag{14}$$

where $\mathscr{V}$ is the reduced volume enclosed by one-half of the boundary, i.e., $\mathscr{V} = V/(2l^3)$, where V is the total physical volume taken up by the relativistic fluid. This is written in this manner, because reflection symmetry as well as axisymmetry is involved, and the zones stretch only from $z = 0$ ($i = 1$) to $z = z_{\max}$ (where $r = 0$, $i = n$). The final equations, which merely serve to keep the entire set a first-order system, are

$$\frac{dz_i}{d\tau} = U_i^z\,, \qquad \frac{dr_i}{d\tau} = U_i^r\,. \tag{15}$$

Figure 1 is a sketch of this symmetric configuration with the relevant quantities labeled on different zones. Thus, the initial values, starting from the spherical configuration that has led to a radius $X' \sim 0.1xl$, satisfy

$$\sum_{i=1}^{n} da_i = 2\pi\left(\frac{X'}{l}\right)^2; \qquad \mathscr{V} = \frac{2\pi}{3}\left(\frac{X'}{l}\right)^3; \qquad \sum m_i = \frac{M'c^2}{2p_0 l^3}\,.$$

The set of $5n + 1$ differential equations, (12)–(15), are not quite in a form suitable for integration. First we eliminate the surface area of a given segment:

$$da_i = 2\pi r_i(\Delta z_i^2 + \Delta r_i^2)^{1/2}\,.$$

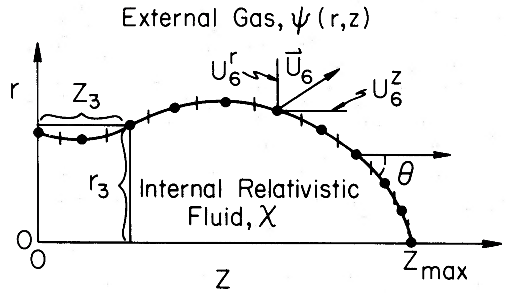

FIG. 1.—The discretized boundary for $n = 11$. Dots indicate the z and r positions of each of the zones at a given time τ. Two velocity components, illustrated at $i = 6$, are also associated with each point as is an angle $\theta = \tan^{-1}(-dr/dz_i)$. Vertical lines demark the boundary of each zone, the surface area and mass contained between them are da_i and m_i, respectively. Note that $i = 1$ and $i = n$ are one-sided and call for special treatment in the code. Physically, the expanding blob has cylindrical symmetry about the z axis and reflection symmetry about the $z = 0$ plane.

Equation (14) harbors three more complex terms. Look first at the kinetic energy:

$$\frac{d(\sum m_i U_i^2)}{d\tau} = \sum \frac{dm_i}{d\tau} U_i^2 + \sum m_i \frac{d}{d\tau} U_i^2$$

$$= \sum \left[\frac{dm_i}{d\tau} U_i^2 + m_i\left(2U_i^r \frac{dU_i^r}{d\tau} + 2U_i^z \frac{dU_i^z}{d\tau}\right)\right] .$$

The change in volume with time and the volume itself are the other aspects still to be considered. $\mathscr{V} = \sum \pi r_i^2 \Delta z_i$ is a simple sum. Then,

$$\frac{d\mathscr{V}}{d\tau} = \pi \sum \left[\frac{dr_i^2}{d\tau} \Delta z_i + r_i^2 \frac{d(\Delta z_i)}{d\tau}\right]$$

$$= \pi \sum \left[2r_i \frac{dr_i}{d\tau} \Delta z_i + r_i^2 \Delta\left(\frac{dz_i}{d\tau}\right)\right]$$

$$= \pi \sum (2r_i U_i^r \Delta z_i + r_i^2 \Delta U_i^z) , \tag{16}$$

where $\Delta U_i^z = (U_{i+1}^z - U_{i-1}^z)/2$, etc.

For any given run in which we have a Gaussian pressure falloff [$\psi(r, z) = \exp(-A_1 r^2 - A_3 z^2)/2$] there are essentially four dimensional parameters and three dimensionless ones. The former may be taken to be L, p_0, l, T (temperature of the confining gas), and the latter as e, α, Γ. When these are combined, the stellar density as well as the gas density are easily found. Of course, the actual initial values of radius and overpressure are needed, but, as mentioned in the previous section, the final results are almost independent of them; to a large extent this is also true of α, but some detailed comparisons will be made below. Throughout our calculations we have taken $\Gamma = 5/3$, correct for a monatomic gas. One further number that should be inserted is the lower limit to the pressure (or density) for the confining gas in intergalactic space. Models have been run for various values of this ultimate density, as well as for the case where it is taken as zero, and the Gaussian drop goes on forever; nontrivial differences result.

c) *A Scaling Law and Preview of Results*

While the simple nondimensionalized strength of a given source is best parametrized by $\mathscr{L} = L/(p_0 l^2 c)$, a useful indication of its strength with additional regard paid to the external medium is $\mathscr{L}' = \mathscr{L}/\beta_s$. Just as $\mathscr{L}'$ is an indication of relative strength, τ' ($\equiv \beta_s \tau$) is a measure of how fast the flow changes in differing external media. From dimensional considerations we expect that a scaling law in $\mathscr{L}'$ and τ' exists. At a specific τ' the shape of two blobs, as well as their sizes in units of their scale heights, will be the same as long as their ($\mathscr{L}'$)s are identical (and as long as e, α, and Γ for the two models are the same). This scaling law was checked for several cases and was verified to a fraction of a percent difference in any variable. Even further, at the same τ' for the same $\mathscr{L}'$, the ratios of E_{ext}/E_{int} will agree, as will those of E_{total}/E_{input}. Note that, by definition, these apply to the entire volume:

$$E_{ext} = \alpha \sum m_i U_i^2 , \qquad E_{int} = 6\pi\chi \sum r_i^2 \Delta z_i , \qquad E_{input} = L\tau , \qquad E_{total} = E_{ext} + E_{int} . \tag{17}$$

Before examining some of the numerical experiments in depth, it may be helpful to glance at the various outcomes of our runs. Because the two dimensionless parameters that convey the most about any given flow are $\mathscr{L}'$

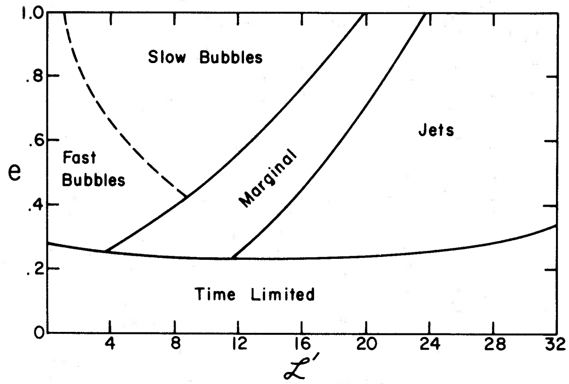

FIG. 2.—General overview of the results of our numerical integrations. The type of outcome is labeled in five regions of the $\mathscr{L}'$ (reduced luminosity)–e (eccentricity of confining gas cloud) plane. See text for details.

and e, we schematically sketch the results of our numerical integrations on an ($\mathscr{L}'$, e)-plane. While we have run about 100 models, many are essentially duplicates, checking the effect of some small change, and our coverage of the plane is sketchy.

The region labeled "jets" in Figure 2 is where we are fairly confident that the plasma escapes in two beams (though not necessarily arriving at the steady state envisioned by BR). In the "bubble" area, the pinching off at the origin should be complete, and two separated blobs seem to form. The further division into "slow" and "fast" bubbles refers to whether or not subsequent plasmoids can catch up with earlier ones. Quite a large swath ("marginal") gives results that appear to go one way or the other, but because of the grossness of our approximations, we hesitate to claim any of the above mentioned fates for the runs falling in this area. "Time limited" means that models with these parameters were not carried out for long enough times to be sure of the outcomes.

IV. NUMERICAL CALCULATIONS

a) *Zoning and Accuracy*

Initial values from the spherical results are used to start off the evolution contained in equations (12)–(15), and the divisions between zones are based on equal separations in arc length. The equations are integrated by the same type of Runge-Kutta routine described above. To preserve a good physical grid, when the boundary elements became too uneven, a rezoning is performed. When the boundary velocity for a given zone becomes subsonic (i.e., U_n, the normal velocity, is less than β_s, the sound speed), mass is no longer being swept up. In lieu of considering the full two-dimensional hydrodynamics involving the compression wave that then propagates ahead of the boundary, we note that the slow moving wall still imparts energy to the external gas, and to aid the stability of the integration scheme, we employ

$$\left.\frac{dm_i}{d\tau}\right|_{\text{new}} = \left(\frac{U_n}{\beta_s}\right)^2 \left.\frac{dm_i}{d\tau}\right|_{\text{old}}, \tag{18}$$

where $(dm_i/d\tau)|_{\text{old}}$ is found from equation (12), but $(dm_i/d\tau)|_{\text{new}}$ is then utilized in equations (13) and (14). If the internal pressure falls below the external pressure in the equatorial region, the motion in that area may be reversed into a contraction, even while the expansion may be reaccelerating in the polar zones. The external gas is assumed to flow downward to continue to supply pressure, but the velocity of the contraction is clearly limited by the external sound speed.

The accuracy of the integrations was checked in several ways. By modifying the external density gradients, or by releasing all the energy over a short time to mock up an explosion, the code was able to reproduce *various* self-similar solutions (Sedov 1959) quite well. The number of zones was also changed, and in going from 100 down to 25 grid points, positions, velocities and energy densities varied by less than 1%. Also, while equation (14) does depend on total energy conservation, we do not have a particular constraint on our equations that forces the total available energy to equal the total inputted energy. Thus the result that the ratio $E_{\text{tot}}/E_{\text{input}}$ varied from unity by less than 3% for nearly all runs, and by less than 0.5% for the majority of them, is quite encouraging.

Unfortunately we do not have any full, multidimensional hydrodynamic calculations related closely enough to our models to provide a satisfactory check. In treating nonspherical supernova explosions, Chevalier and Gardner (1974) compare a similar thin-wall approximation (where, however, they assume a constant ratio of postshock pressure to internal pressure taken from the spherical case) to a couple of two-dimensional hydrodynamic models. They find that the approximate calculations exaggerate nonspherical effects, and in translating this to our approach

TABLE 1

INPUT AND RESULTS FOR $e = 0.50$ NUMERICAL INTEGRATIONS

Run No. (1)	L_{46} (2)	$\mathscr{L}'$ (3)	α (4)	τ_{end} (5)	z_{end} (6)	r_{end} (7)	Comments (8)
75.............	0.05	0.334	2	209	0.675	0.384	Figs. 3 and 4
73.............	0.20	1.337	2	260	1.150	0.673	Table 4
47.............	0.50	3.343	1	314	1.741	1.049	Cf. next 3 entries
53.............	0.50	3.343	2	309	1.702	1.020	
54.............	0.50	3.343	3	306	1.671	0.999	Table 4
55.............	0.50	3.343	4	303	1.648	0.969	
59.............	1.00	6.686	2	372	2.501	1.528	Table 4
85.............	2.00	13.372	2	766	12.838	6.732	Table 4, $n^* = 5\,(-4)$
42.............	5.00	33.430	1	941	39.127	13.762	"blast" Figs. 3 and 4

their results might imply that a larger α should be used at lower Z values, but we have not attempted such modifications. Sanders (1976) considers strong explosions in galactic nuclei using another two-dimensional code, and his "Explosion 1" is in some respects comparable to several of our high-eccentricity runs. In particular, the shape and size (when divided by scale heights) agree quite well with our run 34 or 35; however, his scaled energy (in units of $P_0 l^3$) is ~ 440, while ours ($E \approx \mathscr{L}\tau$) is only ~ 57. But the comparison should be made in terms of $\mathscr{L}'$ and τ', and the value of $\mathscr{L}'$ for Sanders's explosion is 2.8×10^3 (using $L = E/t_{\rm breakout}$), almost a factor of 100 higher than any we considered.[1] It should also be noted that since we assume a constant luminosity, not an explosion, as well as higher temperatures and a relativistic fluid, we should expect results somewhat different from any previous work.

The numerical computations are terminated when the boundary velocities start to become relativistic or the $p = p(t)$ assumption begins to fail. We ignore such a failure if due to pinching off at the center, and brazenly continue to evolve the system as a pair of bubbles. A detailed discussion of the termination criteria would absorb too much space (Wiita 1976); suffice it to say that almost always a run was ended by the expansion going relativistic in some zones.

b) *The Early Stages: No Bubbles*

Within any large category of calculation types, the three parameters L, e, and α are the ones of most interest, and runs were made for several values of each. The strength of the energy source, L, was found to be crucial in determining when and if bubbles would form, and if there was enough energy to blast out jets in the polar directions. Contrary to the supposition of BR, but in agreement with others dealing with somewhat similar problems (e.g., Sakashita 1971), not much collimation could be achieved unless a rather large value for the potential's eccentricity was assumed. Finally, it was interesting to note that the value of α, which was allowed to equal 1, 2, 3, or 4, had surprisingly little effect on the overall shape, or on the time at which bubbles would form, for example. Furthermore, the scaling law of § III*c* was tested and found justified (cf. runs 34 and 35 in Table 3).

We now marshal about 30 of the more than 100 actual runs of the program. Given in Tables 1, 2, and 3 are certain useful results pertaining to calculations based on the "canonical" BR parameters for Cyg A; thus, unless stated otherwise in the Comments column (8), all the runs have in common the following data: $l = 135$ pc, $X_0 = 0.01l$, $p_{0-4} = 0.3$, $T_8 = 3$, $\beta_s = 0.0096$, and the intergalactic number density is taken as $n^* = 0.0$. Either 20 or 25 points along the boundary are used in all tabulated cases. Table 1 shows nine relatively flat runs, those with

[1] I thank the referee for suggesting these comparisons.

TABLE 2

INPUT AND RESULTS FOR INTERMEDIATE ECCENTRICITY NUMERICAL INTEGRATIONS

Run No. (1)	L_{46} (2)	$\mathscr{L}'$ (3)	α (4)	τ_{end} (5)	z_{end} (6)	r_{end} (8)	Comments (8)
				$e = 0.75$			
67.............	0.50	3.343	2	263	1.657	0.950	Table 4
83.............	3.00	20.058	2	673	17.685	7.728	Table 4, $n^* = 5\,(-4)$
				$e = 0.90$			
48.............	0.50	3.343	1	233	1.657	0.926	Cf. run 67
65.............	1.00	6.686	2	267	2.274	1.258	Table 4, Figs. 3 and 4
78.............	2.50	16.715	2	362	5.487	2.366	
86.............	3.00	20.058	2	463	12.633	4.839	Table 4, $n^* = 5\,(-4)$

TABLE 3

INPUT AND RESULTS FOR $e = 0.999$ NUMERICAL INTEGRATIONS

Run No. (1)	L_{46} (2)	$\mathscr{L}'$ (3)	α (4)	τ_{end} (5)	z_{end} (5)	r_{end} (7)	Comments (8)
71........	0.05	0.334	2	123	0.603	0.316	Table 4
43........	0.10	0.669	1	139	0.800	0.417	Fig. 7
69........	0.20	1.337	2	155	1.036	0.552	$n^* = 5\,(-4)$
45........	0.50	3.343	1	184	1.576	0.831	Table 4
46........	1.00	6.686	1	214	2.453	1.156	
44........	2.00	13.372	1	251	6.358	1.784	Cf. next 3 entries
51........	2.00	13.372	2	246	4.479	1.607	
50........	2.00	13.372	3	242	3.882	1.497	
52........	2.00	13.372	4	237	3.440	1.426	
39........	3.00	20.058	1	209	5.176	1.502	"blast" Fig. 5
80........	4.00	26.744	2	276	26.049	6.164	"blast"
84........	5.00	33.430	2	342	34.482	19.423	Table 4, $n^* = 5\,(-4)$, Figs. 3, 4, 7
34........	5.00	33.430	1	179	5.489	1.597	$p_{0-4} = 1.2$, $l = 67.5$ pc
35........	5.00	33.430	1	354	5.400	1.574	"blast," $p_{0-4} = 0.6$, $T_8 = 0.75$

$e = 0.50$; column (1) gives the run number for identification purposes; the most important parameter, the luminosity (in units of 10^{46} ergs s^{-1}) is given in column (2), and its reduced value, $\mathscr{L}'$, is in column (3). The value of α used in that particular model is listed in column (4). The values of τ, z_{max}, and r_{max} at the time each run (or the non–bubble-like phase of the run) ended are stated in columns (5), (6), and (7), respectively. Table 2 provides the same information for six runs of intermediate eccentricity, while Table 3 tells us about 14 cases where the gas is very flattened. Putting dimensions back in, we recall that $\tau = 1$ implies l/c seconds have gone by, and for the value of l used for essentially all these cases, this leads to the conversion: $\tau = 1 = 1.39 \times 10^{10}$ s $= 442$ yr; also, the values for z and r are quoted in terms of l: 135 pc $= 4.166 \times 10^{20}$ cm. Most of the runs listed in these tables terminated (at least for this stage) with bubble formation; and if no comment is present, this is to be assumed. The notation "blast" in column (8) means that the calculation went nonrelativistic and appeared to be sending out jets before pinching off, while "time" indicates that the best run was terminated by exceeding a fixed initial temporal bound on the evolution. Finally, "$p < 0$" means that our approximations were sufficiently crude that carrying the integration out beyond the τ_{end} listed leads to the evolution equations implying a negative internal pressure; although this caused a termination in the code, one really expects that when the pressure does get very low, the boundary will start to implode all over or, more probably, fragment, since the thin wall approximation becomes useless, and the wall material would expand inward.

With all other variables held constant, we find that the times at which various similar facets of the evolution occurred varied very little with α. Averaging comparisons made for six different (L, e) combinations, we find a weak dependence, summarized by

$$\frac{1}{\tau_{end}} \frac{\partial \tau_{end}}{\partial \alpha}\bigg|_{L,e} \approx -0.015 \pm 0.004 \text{ (formal 1 } \sigma \text{ spread)}\,. \tag{19}$$

Obviously, the value of α does change the ratio of the amount of energy stored in the walls (kinetic plus internal) to that residing in the relativistic plasma.

Now we examine in more detail a sample of five of the runs we have tabulated: they can be characterized on a strength-eccentricity grid as follows: run 75, weak and spherical; run 42, strong and spherical; run 65, intermediate and moderately flattened; run 69, weak and flat; run 84, strong and flat. Figure 3 presents the values of χ, the ratio of our assumed constant-in-space internal pressure, to the central pressure of the confining gas, plotted on a log-log scale against the nondimensionalized time τ.

We draw the following conclusions from Figure 3. First, the initial value of the overpressure (equivalently, initial velocity) is not important. Second, between $\tau = 1$ and $\tau \approx 30$, the slopes are rather constant, as the blobs expand almost spherically: approximately, $\chi \propto \tau^{-0.7}$. Also, once χ falls below one, the drop becomes much more precipitous, with expansion losses dominating the injected energy (which is cut off if the blob bifurcates).

The maximum elongation in the polar direction, z, as well as the radius of the first zone, r, are given as functions of τ for the same five runs in Figure 4. If and when r goes to zero, we declare that a bubble has formed, and in its stead we commence plotting z_{min}, the rear surface of the bubble. A comparison of runs 65 and 69 (Fig. 4*b*) shows how the stronger source, 65, has a larger radius at any given time, and its lower eccentricity enables it to avoid showing much asphericity until $\tau \approx 100$. The differences between cases 42 and 84 (Fig. 4*c*) are dominated by the fact that run 84 has a lower bound on the intergalactic density, while run 42 does not.

Another way of presenting the output of some of these numerical investigations is to show snapshots of the entire shape at specific times. Consider run 39, which we have not yet discussed in any detail; it is depicted in Figure 5, which gives the shape of the wall at the labeled times in one quadrant. A rotation about the z-axis and

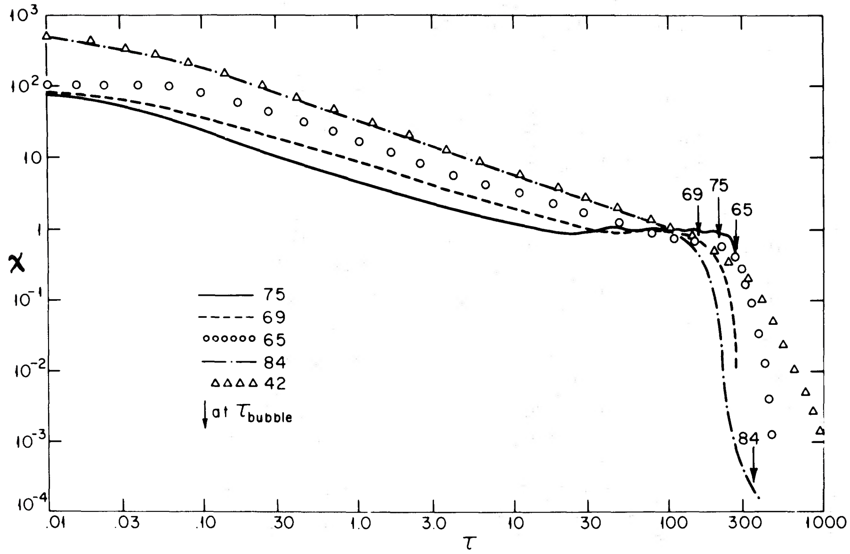

FIG. 3.—Internal pressure as a function of dimensionless time for five cases. Run 75 ($L_{46} = 0.05$, $e = 0.50$, $\alpha = 2$) follows the solid line. Run 69 ($L_{46} = 0.20$, $e = 0.999$, $\alpha = 2$) is shown by the dashed line. Run 65 ($L_{46} = 1.0$, $e = 0.90$, $\alpha = 2$) follows the circles. Run 84 ($L_{46} = 5.0$, $e = 0.999$, $\alpha = 2$) goes along the dot-dash line. Run 42 ($L_{46} = 5.0$, $e = 0.50$, $\alpha = 1$) has a pressure drop that follows the triangles.

a reflection about the $z = 0$ plane would yield the entire volume. This is a flat ($e = 0.999$) and quite powerful ($\mathscr{L}' \approx 20$) model which displays a substantial amount of collimation by the time $\tau = 209$, when the polar expansion is semirelativistic and accelerating. Since U^r is already negative and this squeezing is also going faster, there is still the possibility that it would pinch off before a real blast is formed, so we must call this a marginal jet formation.

c) *Bubbles and Compact Parameter Sets*

We have just seen how, for most values of eccentricity and luminosity we have considered, a neck tends to form and pinch off, at least as long as we utilize our approximations and neglect the feedback from the central energy source. After the innermost zone has pinched off, subsequent zones near the trailing edge smash into the axis; we then divorce them from the rest of the calculation. This would physically imply that the bubbles move outward, leaving a tail of denser material behind them. Of course, this is not a good picture, the blobs being more likely to sweep material out of the way (Christiansen 1973) than to add some; but since these inner zones usually have a small fraction of the energy, the errors so introduced are not substantial. As opposed to the necessarily subsonic and buoyancy-driven bubbles of Gull and Northover (1973), our bubbles are primarily pushed and distorted by the pressure differential across both their leading and trailing boundaries, and they can move supersonically at the former.

Eleven models that formed bubbles are drawn from Tables 1 through 3 and are listed in Table 4. The first four columns are purely reidentification. Now τ_{end} refers to the final termination of the run, with the beginning of the

TABLE 4

SELECTED BUBBLE-FORMING NUMERICAL EVOLUTIONS

Run No. (1)	e (2)	L (3)	α (4)	τ_{end} (5)	z_{max} (6)	z_{min} (7)	r_{max} (8)	Comments (9)
73......	0.500	0.20	2	650	3.655	2.787	1.074	"time"
54......	0.500	0.50	3	2791	29.289	16.262	8.774	"time"
59......	0.500	1.00	2	586	5.539	2.360	2.695	"$p < 0$"
85......	0.500	2.00	2	955	20.572	1.593	10.460	"$p < 0$," $n^* = 5\ (-4)$
67......	0.750	0.50	2	605	5.766	3.173	1.970	"time"
83......	0.750	3.00	2	1009	43.674	3.443	17.993	"time," $n^* = 5\ (-4)$
65......	0.900	1.00	2	461	7.361	1.779	2.549	"$p < 0$," Figs. 3, 4, 6
86......	0.900	3.00	2	1030	51.978	5.644	24.513	"time," $n^* = 5\ (-4)$
71......	0.999	0.05	2	1017	16.929	10.077	3.399	"time"
45......	0.999	0.50	1	338	11.737	2.026	1.962	"blast"
84......	0.999	3.00	2	390	39.452	2.052	25.938	essentially blast $n^* = 5\ (-4)$, Figs. 2, 4

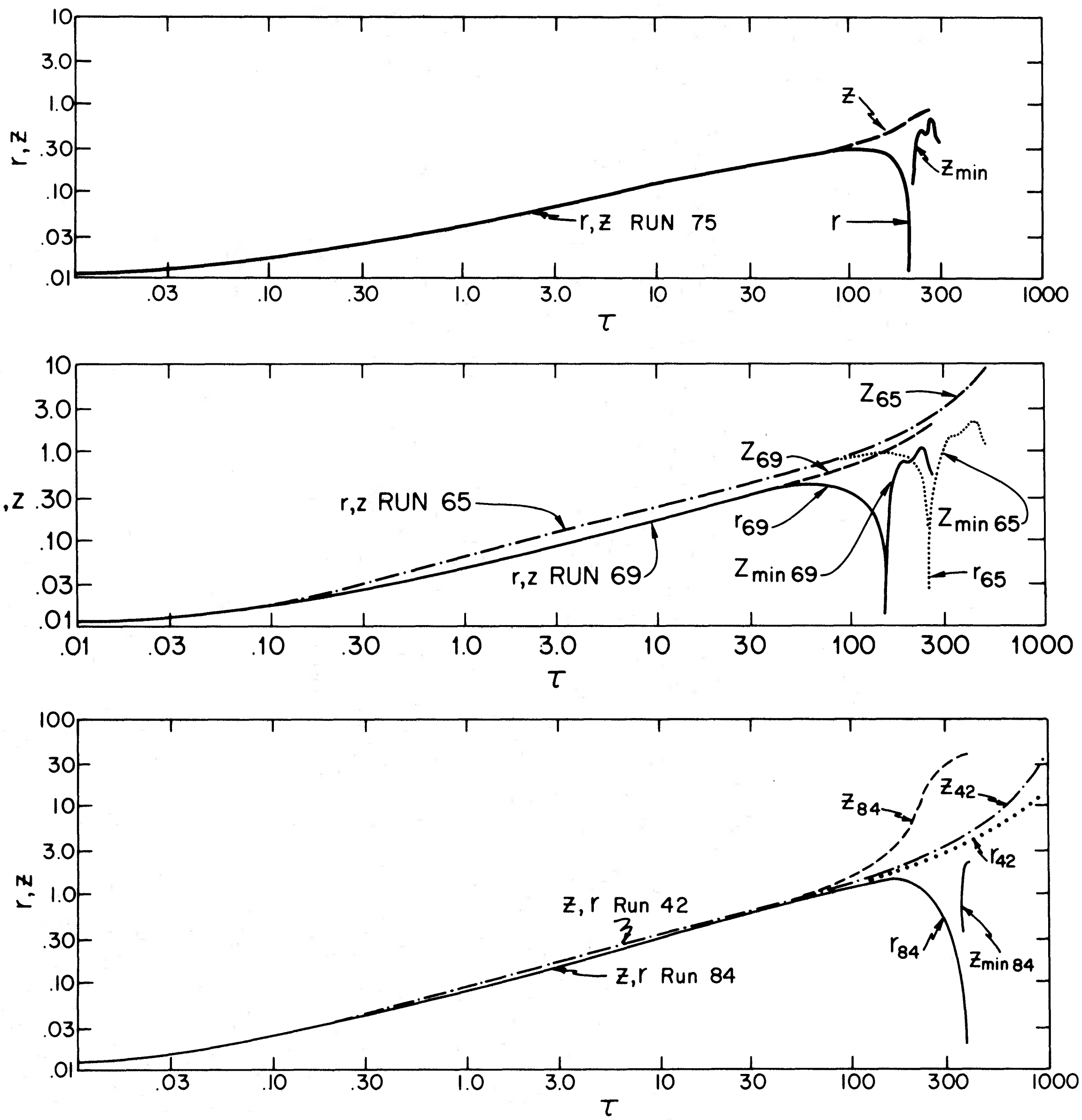

FIG. 4.—Radii of the first zone and z-coordinates of the last zone as functions of time: (a) For run 75 the solid line is the r value and the dashed curve is the z value. After $r = 0$, the solid line gives the rear boundary of the bubble. In (b), run 69 is just as for run 75 in (a). For run 65, in (b), the dash-dot line gives the maximum z value, and the dotted curve gives the radius, then the rear of the bubble. Run 84 is depicted in (c) just as run 69 is in (b). For run 42, just as run 65 above, except that r never goes to zero.

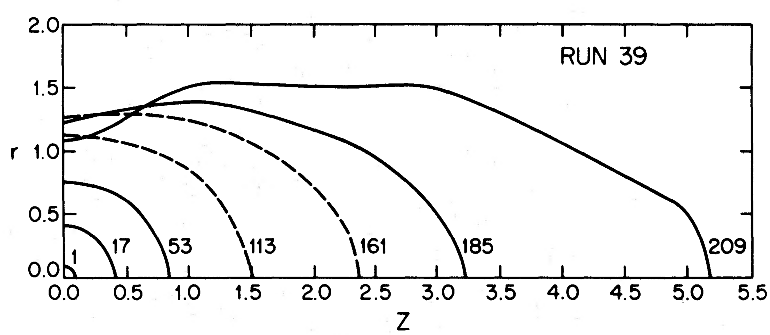

FIG. 5.—The boundaries of the relativistic fluid for run 39 ($L_{46} = 3.0$, $e = 0.999$, $\alpha = 1$) in one quadrant as a function of time. The labels next to the curves are the time in units of l/c.

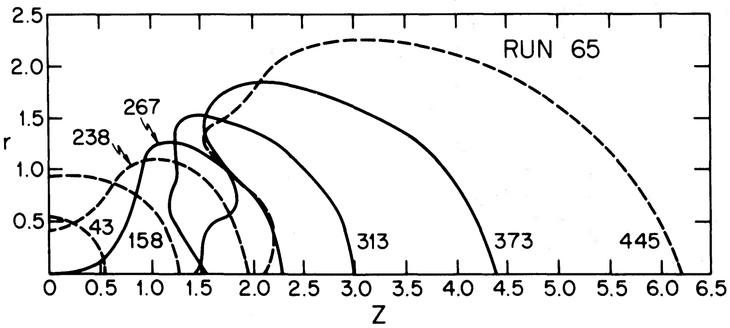

FIG. 6

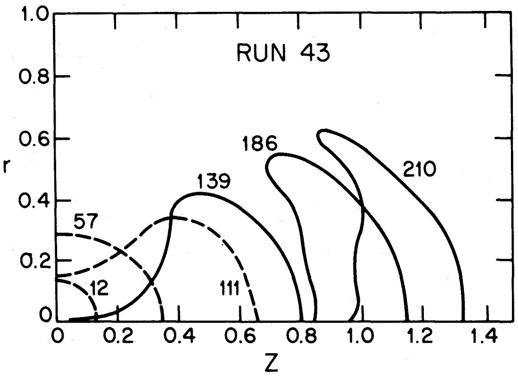

FIG. 7

FIG. 6.—As in Fig. 5 for run 65 ($L_{46} = 1.0$, $e = 0.90$, $\alpha = 2$)
FIG. 7.—As in Fig. 5 for run 43 ($L_{46} = 0.1$, $e = 0.999$, $\alpha = 2$)

bubble phase being given by the τ_{end} (col. [5]) for the same run in its earlier tabular appearance. At that late time (this new τ_{end}) the values for the maximum and minimum extent along the polar axis as well as the largest radial dimension of each packet of plasma, are given in columns (6), (7), and (8). Column (9) contains comments, with the termination code words the same as those in the previous section.

We can classify the various cases on a "fast"–"slow" spectrum. "Fast" bubbles are those that seem to rise sufficiently rapidly that by the time a new bubble is ready to break off, the earlier one is far removed from the origin; "slow" ones can be caught by younger siblings. Runs 73, 54, and 71 can be classified as fast, while runs 85, 83, 65, 86, and 84 are slow; the others (59, 67, 45) are intermediate in speed. It is clear that the fast runs come from the weakest sources while the slow ones arise from more powerful sources. A finite minimum external density also tends to slow the escape of earlier bubbles. Overall, we confirm the idea of Christiansen (1973) and Gull and Northover (1973) that later bubbles can catch up with, and probably merge with, earlier ejecta. The possibility mentioned in Blandford and Rees (1975) of a stream of bubbles coalescing into a jet thus also remains a viable alternative model for jet formation.

Run 65 has already been discussed in considerable detail; thus, a perusal of Figure 6 should be adequate to detect the salient features of this "slow" type. We see that the trailing boundary advances much less rapidly than does the leading one, and a new bubble that starts to form at $\tau = 267$ when this one is ejected would probably catch up with this one around $\tau = 550$. Figure 7 depicts a "fast" case, run 43. Here the bubble's irregular rear boundary quickly approaches a rather stable fraction of the smooth front boundary.

Six numerical experiments were performed using parameters characteristic of the smaller galactic nuclei models of Paper I. The results paralleled those already presented for the cooler, less dense, clouds. Variations due to eccentricity and luminosity go the same way; and the ($\mathscr{L}'$, τ') scaling law is verified over a very wide range. No difference is seen in terms of stability or ease of nozzle formation, so the relative strengths and weaknesses of the models remain as described in Paper I.

V. CONCLUSIONS

Several of the results we have found could have been expected, but the actual relationships should be summarized. The larger the eccentricity of the confining potential, the better collimated the expanding jets are, and the sooner a bifurcation into bubbles occurs. Obviously enough, increasing the power of the mass-energy source makes for a larger volume at a given time, all else being equal. Figure 8 demonstrates these relationships by showing the time at which bubbles form (for $\alpha = 2$ runs) plotted against L; different lines correspond to different values of e.

Such an increase in luminosity also postpones the choking off at the origin; and for a sufficiently powerful source, a blast out rather than a bifurcation is the likely outcome. However, this value of $L_{46} \approx 2.5$ is considerably higher than what the basic stationary models call for. A way to incorporate both results is to assume that at early times a more powerful source carved out a channel which then relaxed into a shape that accommodates the present, less powerful, momentum flux. Again, the grossness of the approximations we have employed should be pointed out, so that such a two-phase scenario may not even be necessary. Despite the results we have obtained, which argue against a wholehearted acceptance of the twin-exhaust model, we have already mentioned at least two other ways in which throats might still be formed. The first of these is due to the likelihood that as the walls recollapse near the center, the pressure gradients will build up and halt them before a division takes place. The other possibility involves slow bubbles being overtaken by, and merging with, later ones to form a channel.

Within the framework of this paper the next step would be to get the coupled flow in the one-dimensional, but relativistic, approximation working. Then the models we have looked at could be followed to much later times.

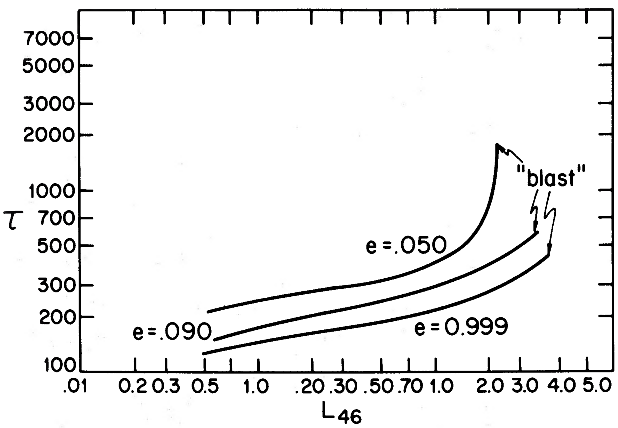

FIG. 8.—Times of bubble formation versus luminosity for differing eccentricities (for canonical BR parameters)

Single jet sources might also be formed if the luminosity source is off center with respect to the confining gas (cf. Chevalier and Gardner 1974). But of course, major progress on this problem demands the discarding of many of our approximations and the employment of a full, two-dimensional magnetohydrodynamic code. However, our approach allows a wider exploration of the ($\mathscr{L}'$, e)-plane than such a more detailed—but also far more costly—method would permit, and thus serves as a guide for such future work.

It is a pleasure to thank William Press, my advisor at Princeton, for many useful suggestions and for supplying encouragement when it was most needed. Conversations with Roger Blandford, Martin Rees, and Craig Sarazin were of substantial help. This work was supported in part by NSF grants GP-30799X at Princeton and AST 74-21216 at Chicago.

REFERENCES

Bhowmick, J. B. 1975, *Ap. Space Sci.*, **35**, L35.
Blake, G. M. 1972, *M.N.R.A.S.*, **156**, 67.
Blandford, R. D., and McKee, C. F. 1976, *Phys. Fluids*, **19**, 1130.
Blandford, R. D., and Pringle, J. E. 1976, *M.N.R.A.S.*, **176**, 443.
Blandford, R. D., and Rees, M. J. 1974, *M.N.R.A.S.*, **169**, 395 (BR).
———. 1975, *Contemp. Phys.*, **16**, 1.
Bollea, D., and Cavaliere, A. 1976, *Astr. Ap.*, **46**, 219.
Chevalier, R. A. 1974, *Ap. J.*, **188**, 501.
Chevalier, R. A., and Gardner, J. 1974, *Ap. J.*, **192**, 457.
Christiansen, W. A. 1973, *M.N.R.A.S.*, **164**, 211.
Cox, D. P., and Daltabuit, E. 1971, *Ap. J.*, **167**, 113.
Cox, D. P., and Tucker, W. H. 1969, *Ap. J.*, **157**, 1157.
Ferrari, A., Trussoni, E., and Zaninetti, L. 1977, *Astr. Ap.*, in press.
Fomalont, E. B., and Miley, G. K. 1975, *Nature*, **257**, 99.
Gear, C. W. 1971, *Numerical Initial Value Problems in Ordinary Differential Equations* (Englewood Cliffs: Prentice Hall).
Gull, S. F., and Northover, K. J. E. 1973, *Nature*, **244**, 80.
Kellermann, K. I., Clark, B. G., Niell, A. E., and Shaffer, D. B. 1975, *Ap. J. (Letters)*, **197**, L113.
Landau, L. D., and Lifshitz, E. M. 1959, *Fluid Mechanics* (Reading: Addison-Wesley).
Longair, M. S., Ryle, M., and Scheuer, P. A. G. 1973, *M.N.R.A.S.*, **164**, 243.
Lumbach, D. D., and Probstein, R. F. 1969, *J. Fluid Mech.*, **35**, 53.
Möllenhoff, C. 1976, *Astr. Ap.*, **50**, 105.
Pauliny-Toth, I. I. K., *et al.* 1976, *Nature*, **259**, 17.
Rees, M. J. 1971, *Nature*, **229**, 312 and 510.
———. 1976, *Comments Ap.*, **6**, 113.
Sakashita, S. 1971, *Ap. Space Sci.*, **14**, 431.
Sanders, R. H. 1976, *Ap. J.*, **205**, 335.
Scheuer, P. A. G. 1974, *M.N.R.A.S.*, **166**, 513.
Sedov, L. I. 1959, *Similarity and Dimensional Methods in Mechanics* (New York: Academic Press).
Spitzer, L. 1968, *Diffuse Matter in Space* (New York: Interscience).
Turland, B. D., and Scheuer, P. A. G. 1976, *M.N.R.A.S.*, **176**, 421.
Wiita, P. J. 1976, unpublished Ph.D. thesis, Princeton University.
———. 1978, *Ap. J.*, **221**, 41 (Paper I).
Zel'dovich, Ya. B., and Raizer, Ya. P. 1966, *Physics of Shock Waves and High Temperature Hydrodynamic Phenomena* (New York: Academic Press).

PAUL J. WIITA: Institute of Astronomy, Madingley Road, Cambridge CB3 0HA, England